



# Fast rigorous mask model for extreme ultraviolet lithography

**ZINAN ZHANG,<sup>1,2</sup> SIKUN LI,<sup>1,2,3</sup> XIANGZHAO WANG,<sup>1,2,4</sup> AND WEI CHENG<sup>1,2</sup>**<sup>1</sup>*Shanghai Institute of Optics and Fine Mechanics, Chinese Academy of Sciences, Shanghai 201800, China*<sup>2</sup>*University of Chinese Academy of Sciences, Beijing 100049, China*<sup>3</sup>e-mail: lisikun@siom.ac.cn<sup>4</sup>e-mail: wxz26267@siom.ac.cn*Received 5 June 2020; revised 24 July 2020; accepted 24 July 2020; posted 24 July 2020 (Doc. ID 399323); published 20 August 2020*

The calculation of extreme ultraviolet (EUV) mask diffraction spectrum is the key of EUV lithography simulation. In this paper, a fast rigorous EUV mask model is proposed to calculate the diffraction spectrum fast and accurately. Based on the mask structure decomposition method, the relationship among the region diffraction, the boundary diffraction of the absorber, and the direction of incident light is analyzed at first. Then the frequency-domain functions related to angle of incidence and diffraction angle are established to model the geometrical and boundary diffraction of the absorber. The fast rigorous EUV mask model is established by combining the equivalent layer multilayer model based on the Fresnel formula and the accurate absorber model. Simulations and comparisons show the effectiveness of the proposed model. For the 14 nm vertical line-space pattern, the calculation errors of critical dimension (CD) via the proposed model are reduced by 80.6% and 93.9% compared with the structure decomposition method for dense and isolate features. © 2020 Optical Society of America

<https://doi.org/10.1364/AO.399323>

## 1. INTRODUCTION

Extreme ultraviolet (EUV) lithography uses EUV light as the exposure source, so that the resolution of single exposure is higher than that of deep ultraviolet (DUV) lithography. It has been applied to the high-volume manufacturing (HVM) of a 7 nm node integrated circuit, and will be the mainstream of a 5 nm node below [1]. Computational lithography techniques, such as optical proximity correction (OPC) and source mask optimization (SMO), are important tools to improve the lithography imaging performance [2–6]. The EUV imaging model needs to be called on repeatedly during the iteration process of OPC and SMO, so the speed and accuracy of the imaging model significantly impact the speed and performance of computational lithography techniques. Meanwhile, researchers of the new EUV machine and lithography process also need a high-precision imaging model as an auxiliary analysis tool. The fast and accurate calculation of EUV mask diffraction spectrum is the key to EUV imaging model [7]. Different from the DUV mask, EUV mask adopts the reflective design with thickness reaching hundreds of nanometers, which is far larger than the wavelength of incident light. Due to the oblique incidence configuration and thick mask effect, the traditional Kirchhoff thin mask model is no longer accurate. It is necessary to apply rigorous electromagnetic simulation techniques, such as the finite difference time domain (FDTD) method and the rigorous coupled wave analysis (RCWA) method, to the EUV mask

simulation [8,9]. However, with the large time and memory consumption, the rigorous methods are not applicable in large-area mask simulation and advanced computational lithography techniques such as SMO.

In order to improve the speed of EUV mask simulation, a series of fast mask models are proposed, including mainly models based on pattern decomposition and models based on structure decomposition. The domain decomposition method (DDM) is a typical fast model based on pattern decomposition [10]. The diffraction spectrum and near-field of the EUV mask can be calculated fast by the DDM, which transforms the complex two-dimensional (2D) pattern into the superposition of a series of one-dimensional (1D) patterns [11]. ASML proposed a fast EUV mask model called M3D+, which decomposes the mask pattern into regions, edges, and corner points. The corresponding filters are obtained in advance by rigorous simulations, and can be used for calculating the aerial image of an arbitrary mask pattern [12]. The structure decomposition method (SDM) decomposes the mask structure into the absorber and multilayer and models them respectively. The diffraction spectrum of mask is calculated by simulating the propagation of incident light. With clear physical meaning, the SDM has been successfully used in the theoretical analysis of mask three-dimensional (3D) effects [13].

The oblique incidence configuration is the dominating reason for the shadowing effect and focus shift effect in the EUV

imaging system [14]. The fast mask models based on pattern decomposition mainly adopt the library method to calculate the mask diffraction spectrum accurately under oblique incidence. The edge-DDM model proposed by Mailfert obtains the DDM signals of pattern edges by rigorous simulation under different polarizations and angles of incidence. By storing the signals as a library in advance, the model can get edge signals quickly by a lookup table and calculate the near-field of a complex mask pattern [15]. The M3D+ model adopts a similar method to obtain the filters of regions, edges, and corners. However, the library method needs to calculate numerous data and makes several assumptions regarding the mask shapes, such as edge angles, feature sizes, and corner sizes. This imposes limitations of the accuracy of the method when dealing with random features [16]. The fast models based on the SDM can directly calculate the mask spectrum under oblique incidence without the pre-recorded library and has higher adaptability to random mask patterns [17]. However, the SDM adopts point pulses to describe the boundary diffraction of absorber pattern edges. The point pulse is a constant that is only related to the absorber material and thickness. It cannot describe the impact of the incidence angle on the absorber diffraction spectrum. Meanwhile, the region diffraction under oblique incidence is simply regarded as the Hopkins shift of diffraction under normal incidence in the model. So the accuracy of the SDM decreases with the increase of the incidence angle and the decrease of the half-pitch of the mask feature.

In this paper, the influence factors of the absorber diffraction spectrum are studied. Rigorous simulations via RCWA show

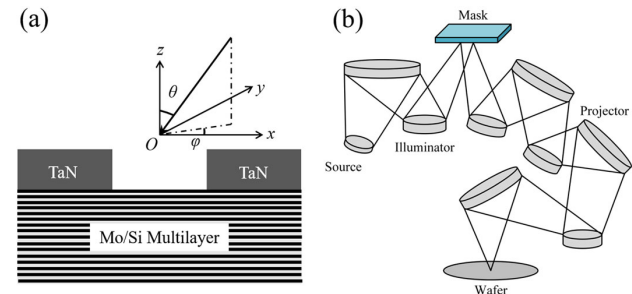


**Fig. 1.** Diagram of (a) EUV mask structure, and (b) EUV imaging system.

represents the angle between the incident light and the  $z$ -axis, and azimuth  $\varphi$  represents the angle between the  $x$ -axis and the projection of incident light on  $xOy$  plane. The absorber and multilayer are respectively modeled by the SDM. The diffraction spectrum of the absorber is calculated by the Kirchhoff thin mask model, which is modified by point pulses, and a phase propagation is added to match the rigorous simulation results. The reflectivity of the multilayer is calculated by the EL model, which is based on Fresnel formula to calculate the transmission and reflection layer by layer [18]. The EL model can be considered as a rigorous model when the multilayer defect is out of consideration. It can accurately obtain the multilayer reflectivity with high speed. The mask spectrum is the superposition of the second absorber diffraction of different diffraction lights.

Taking a 1D line-space pattern as an example, the analytical expression of the SDM [13] is as follows:

$$\begin{aligned} E(\alpha_n, \beta_n) &= \int E_{\text{absorber}}(\alpha_{\text{in}}, \beta_{\text{in}}, \alpha_m, \beta_m) R(\gamma_m) E_{\text{absorber}}(\alpha_m, \beta_m, \alpha_n, \beta_n) d\alpha_m d\beta_m \\ E_{\text{absorber}}(\alpha_{\text{in}}, \beta_{\text{in}}, \alpha_m, \beta_m) &= \Phi_1(\alpha_{\text{in}}, \beta_{\text{in}}) B(\alpha_m - \alpha_{\text{in}}, \beta_m - \beta_{\text{in}}) \Phi_2(\alpha_m, \beta_m) \\ E_{\text{absorber}}(\alpha_m, \beta_m, \alpha_n, \beta_n) &= \Phi_2(\alpha_m, \beta_m) B(\alpha_n - \alpha_m, \beta_n - \beta_m) \Phi_1(\alpha_n, \beta_n), \end{aligned} \quad (1)$$

that, under certain absorber material and thickness configurations, the region diffraction mainly depends on the geometric features of pattern, and the boundary diffraction only depends on the incidence angle as well as the diffraction angle. Fast rigorous simulation can be achieved by accurately describing the relationship between the incidence angle and the absorber diffraction spectrum. Instead of point pulses, frequency-domain functions are established in this paper to accurately describe the impact of the incidence angle on the diffraction spectrum. The influence factors are all accurately modeled in the absorber model to achieve fast and rigorous simulation. Then the fast rigorous EUV mask model is established by combining the equivalent multilayer (EL) model based on the Fresnel formula and the accurate absorber model.

## 2. THEORY

### A. Analysis of SDM

The EUV mask structure and imaging system are shown in Fig. 1. The typical EUV mask is mainly composed of the TaN absorber and the Mo/Si multilayer. The incidence angle  $\theta$

where  $m, n$  represent the diffraction orders;  $\alpha_{\text{in}}, \beta_{\text{in}}$  represent the direction cosine of incident light;  $\alpha_m, \beta_m$  represent the direction cosine of the  $m$ -th order after the first absorber diffraction;  $\alpha_n, \beta_n$  represent the direction cosine of the  $n$ -th order after the second absorber diffraction;  $\gamma_m = \arccos(\sqrt{1 - \alpha_m^2 - \beta_m^2})$  represents the angle between the  $m$ -th diffraction light and the normal direction of the multilayer;  $\Phi_1, \Phi_2$  represent the phase factors from the middle of the absorber to the upper and bottom surface, respectively;  $B$  represents the absorber diffraction spectrum calculated by the pulsed modified thin mask model; and  $R$  represents the reflectivity of the multilayer for different diffraction lights.

Without considering the shift of space pattern, the absorber diffraction spectrum can be calculated by the pulsed modified thin mask model as follows:

$$B_m = t_a \operatorname{sinc}(m) + (t_b - t_a)d \operatorname{sinc}(md) + \frac{2A}{p} \cos(\pi md), \quad (2)$$

where  $t_a, t_b, A$  are model parameters calibrated by rigorous simulation and are only related to the material and thickness of the absorber,  $p$  represents the pitch of the mask and  $d$  represents the

duty cycle of the space pattern. It is worth noting that the diffraction orders or diffraction angles can be considered as continuous distribution because of the analytic expression of the spectrum.

The model parameters should be calibrated via rigorous simulation. With a line-space pattern of certain size/pitch such as 125/250 nm (wafer scale), RCWA is used to calculate the absorber spectrum under the normal incidence and TE/TM polarizations. The calculation results of 0, +1 and +2 diffraction orders are combined with the expression of  $B_0$ ,  $B_{+1}$  and  $B_{+2}$  from Eq. (2) to obtain the  $t_a$ ,  $t_b$ ,  $A$ . Even for the absorber constituted of more than one layer, the model parameters can be estimated by the material complex indexes and thicknesses of all the sub-layers, and calibrated using the same method [19].

The thin mask model modified by point pulses has clear physical meaning. The first term describes the background intensity, with  $t_a$  representing the background transmission of the absorber. The second term describes the region diffraction, whose amplitude distribution is modulated by the duty cycle.  $t_b$  represents the feature transmission of the absorber, which further modulates the amplitude and phase distribution of region diffraction. The third term describes the boundary diffraction. The amplitude distribution of boundary diffraction is a cosine function in the frequency domain after adding two point pulses at the edges of space pattern.  $A$  represents the intensity of point pulse, which modulates the amplitude and phase of boundary diffraction.

With the pulses modification, phase matching, and the superposition of the second absorber diffraction spectrum, the SDM can accurately and quickly calculate the diffraction spectrum of the thick EUV mask. Considering the 1D line-space pattern whose size/pitch is 500/1000 nm, the feature is 125/250 nm at

wafer scale because of the  $4\times$  reduction of imaging system. The features are all described at wafer scale in the following sections. The RCWA method and the SDM are used for calculating the absorber and mask spectrum under TE polarization and a  $6^\circ$  incidence angle; the comparison is shown in Fig. 2. Figures 2(a) and 2(c) show the amplitude and phase of the absorber spectrum. Figures 2(b) and 2(d) show the amplitude and phase of the mask spectrum, including the absorber and the multilayer. The material index and thickness of the absorber and multilayer are clarified in Section 3.A.

With Eq. (2) and Fig. 2(a), we can find that when the duty cycle is 0.5, the even orders of the absorber spectrum represent the boundary diffraction, and the odd orders represent the region diffraction. By using point pulses modification, the SDM sufficiently describes the region and boundary diffraction in a certain range of diffraction angles. Meanwhile, the asymmetry of mask spectrum caused by oblique incidence is achieved by the superposition of the second absorber diffraction spectrum, as shown in Fig. 2(b).

The modulations of the SDM for region and boundary diffraction are constant values in the complex domain. The model parameters remain constant for all diffraction orders with any incidence angle. So the accuracy of absorber model will decrease when the incidence angle increases, which leads to the calculation error of the second absorber diffraction. On the other hand, the intensity of diffraction light with high order will increase when the half-pitch of feature decreases. The constant modulation can no longer accurately describe the diffraction light with a large diffraction angle, which further leads to a decrease of simulation accuracy. Simulation results are shown in Section 3 in this paper.

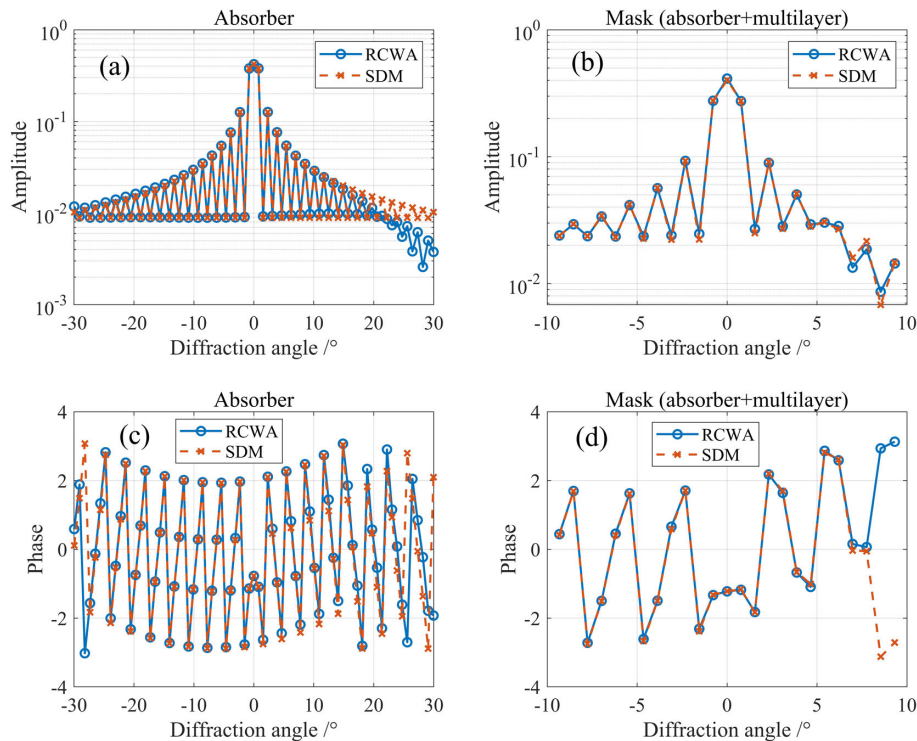


**Fig. 2.** Comparison of SDM and RCWA. (a) Absorber spectrum amplitude. (b) Mask spectrum amplitude. (c) Absorber spectrum phase. (d) Mask spectrum phase.

## B. Construction of the Frequency Domain Functions

In this paper, several frequency domain functions are proposed to improve the accuracy of the fast model. The functions can describe the modulation of absorber for different diffraction orders at any incidence angle, and the absorber spectrum can be calculated by

$$\begin{aligned} B_m &= t_a \text{sinc}(m) + (t_b - t_a) F_{\text{pol}}(\theta_{\text{eq}}, \theta_m) d \text{sinc}(md) \\ &\quad + \frac{2A}{p} G_{\text{pol}}(\theta_{\text{eq}}, \theta_m) \cos(\pi md) \\ \theta_m &= \arcsin\left(m \frac{\lambda}{p}\right), \quad \theta_{\text{eq}} = \frac{\pi}{2} - \arccos(\sin \theta_{\text{inc}} \cos \varphi), \end{aligned} \quad (3)$$

where  $F_{\text{pol}}$ ,  $G_{\text{pol}}$  are frequency domain functions under certain polarization;  $\theta$ ,  $\varphi$  are the incidence angle and azimuth described in Fig. 1(a), respectively; and  $\theta_m$  is the diffraction angle of  $m$ -th order relative to the 0-th order.  $\theta_{\text{eq}}$  is defined as the “equivalent incidence angle,” which determines the distribution of the diffraction spectrum for the 1D mask pattern.

The physical meaning of Eq. (3) is intuitive. The sinc and cosine functions describe the region and boundary diffraction, respectively.  $t_a$ ,  $t_b$ ,  $A$ , which are only related to the material and thickness of absorber, describe the modulation of the absorber on the region and boundary diffraction.  $F_{\text{pol}}$ ,  $G_{\text{pol}}$ , which are related to the incidence and diffraction angle with certain absorber material and thickness, describe the modulation of the absorber on diffraction light with different diffraction angles at any incidence angle. The frequency domain functions are asymmetric under oblique incidence, which means that the function values of positive and negative diffraction angles are not symmetric relative to the zero diffraction order. This will result in the asymmetric diffraction spectrum and near-field, which has peak on the illuminated edge and dip on the shadowed edge. It is almost impossible to obtain the analytical expression of the frequency domain functions, because the traditional rigorous simulation methods calculate the diffraction spectrum by solving the Maxwell differential equation.

It can be seen from the analysis of Eqs. (2) and (3) that the spectrum of certain diffraction orders is generally the superposition of region and boundary diffraction. However, when the duty cycle is 0.5, the region and boundary diffraction spectrum can be separated from each other because of the properties of sinc and cosine functions. The odd orders are region diffraction spectrum and the even orders are boundary diffraction spectrum. In order to obtain the distribution of the frequency domain functions, the duty cycle is set to 0.5 with a certain mask pitch, and the absorber diffraction spectrum needs to be calculated by the RCWA method and the SDM, respectively. Then the even and odd orders, respectively, are extracted. The frequency domain functions are the ratio of the SDM results to rigorous results, as follows:

$$\begin{aligned} F_{\text{pol}}(\theta_{\text{inc}}, \theta_m) &= \frac{B_{\text{odd}}^r}{\Phi_1 B_{\text{odd}} \Phi_2} = f(\theta_{\text{inc}}, \theta_m) \exp[i\phi_f(\theta_{\text{inc}}, \theta_m)] \\ G_{\text{pol}}(\theta_{\text{inc}}, \theta_m) &= \frac{B_{\text{even}}^r}{\Phi_1 B_{\text{even}} \Phi_2} = g(\theta_{\text{inc}}, \theta_m) \exp[i\phi_g(\theta_{\text{inc}}, \theta_m)], \end{aligned} \quad (4)$$

where  $B^r$  is the rigorous simulation result of the absorber, odd, even represent the odd and even diffraction orders,  $f$ ,  $g$  represent the amplitude of frequency domain functions, and  $\phi_f$ ,  $\phi_g$  represent the phase. The distribution of the diffraction spectrum calculated by rigorous simulation is discrete because of the periodic hypothesis, so the ratio values obtained by this method are considered as the sampling of true continuous frequency domain functions. The values can be stored for further calculation. In Eq. (4),  $\Phi_1$ ,  $\Phi_2$  are used for phase matching when calculating the absorber spectrum by the SDM. Thus, the phase of the frequency domain function after the division describes the residual phase error caused by the absorber thickness and the edge diffraction effect. It is worth noting that Eq. (3) can be used for calculating the absorber spectrum with any duty cycle, and that the 0.5 duty cycle is only used for parameters calibration and obtaining the frequency domain functions.

Under the condition that the polarization is TE, and the incidence angles are  $0^\circ$  and  $6^\circ$ , respectively, the mask pitches are set to 250 nm, 100 nm, and 40 nm, respectively. The amplitude and phase distributions of the frequency domain functions obtained by Eq. (4) are shown in Fig. 3. According to Eq. (4), only the absorber needs to be simulated by RCWA and the SDM.

As shown in Fig. 3, the frequency domain functions take the diffraction angle as variable at certain incidence angles. Even if the mask pitch changes, the diffraction lights with the same diffraction angle have the same function values. The distribution of frequency domain functions will vary with the incidence angle.

Similar to the library-based method of the DDM and the M3D+, the frequency domain functions are calculated by the proposed method with a series of incidence angles and are stored as a library. However, the time and space consumption are much less because only the absorber with a duty cycle of 0.5 at certain mask pitch needs to be simulated. Physically, the modulation of the absorber on diffraction light will vary continuously with the incidence angle, so the frequency domain functions at arbitrary incidence angle can be obtained by the interpolation of the library data. Under the condition that the mask pitch is 250 nm, and polarization is TE, the frequency domain functions at  $5.5^\circ$  incidence angle are obtained by the simulation method via Eq. (4) and the interpolation method. According to Eq. (4), the RCWA and SDM are both used for the simulation method. The frequency domain functions at  $5^\circ$  and  $6^\circ$  incidence angles are calculated in advance for interpolation. The comparison is shown in Fig. 4.

Based on the analysis above, a fast and rigorous EUV mask model is proposed in this paper. First, the frequency domain functions are calculated by simulations under TE and TM polarizations with a series of incidence angles, which are from  $-40^\circ$  to  $40^\circ$  with an increment of  $1^\circ$ . Then the function values are stored as a library. The absorber diffraction spectrum

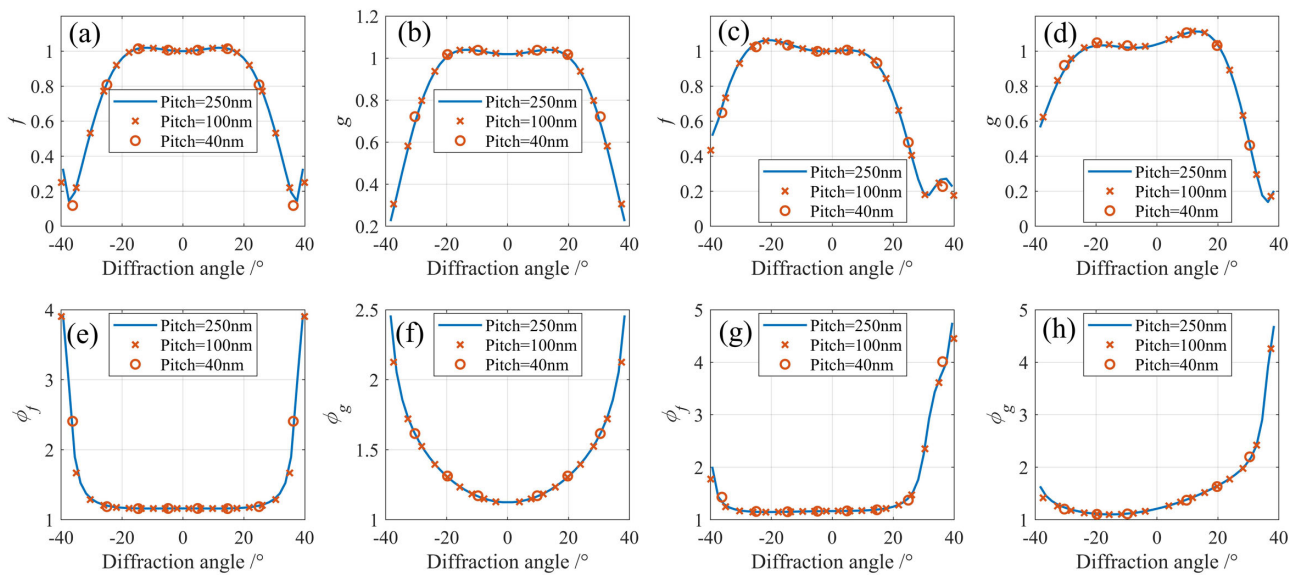


**Fig. 3.** Frequency domain functions under different incidence angles and pitches. Row 1 is amplitude distribution and row 2 is phase distribution; Columns 1–2 are results of 0° incidence angle; columns 3–4 are results of 6° incidence angle.

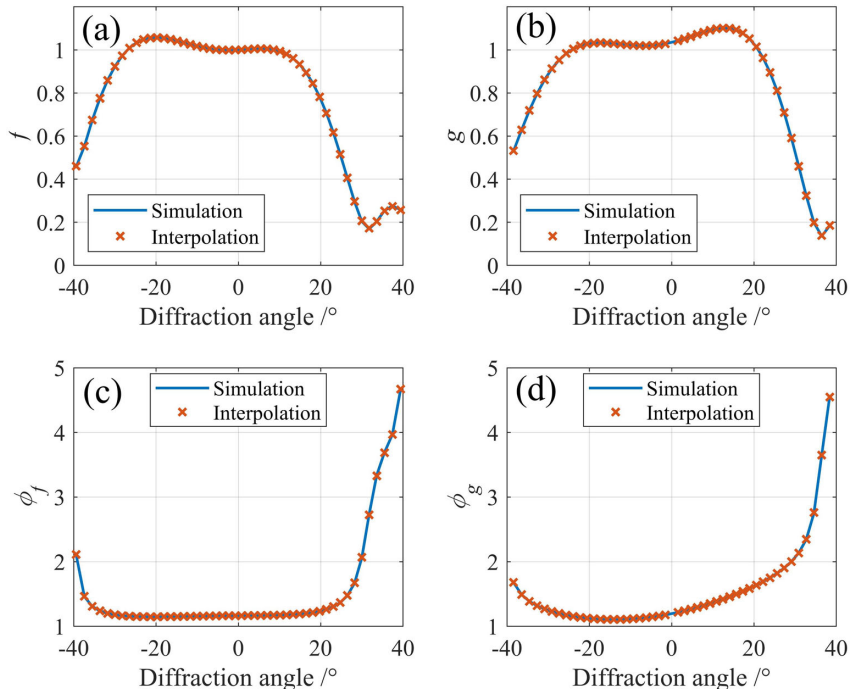


**Fig. 4.** Frequency domain functions obtained by simulation and interpolation under 5.5° incidence angle. (a)–(b) The amplitude of frequency domain functions. (c)–(d) The phase of frequency domain functions.

is calculated by phase matching and Eq. (3), in which the frequency domain functions are obtained by interpolation of the library data. The reflectivity of the multilayer is calculated by the EL model. Compared with the SDM, the proposed method describes the modulation for different diffraction light under different incidence angles via frequency domain functions, which can effectively improve the model accuracy. On the other hand, although the frequency domain functions need to be calculated in advance, only the absorber with a duty cycle of 0.5

at a certain mask pitch needs to be simulated. So the computational burden and complexity are less than with the DDM and M3D+ model. With clear physical meaning, high accuracy, and pretty high speed, the proposed model is reasonable for being considered as a fast, rigorous EUV mask model.

Similar to Fig. 2, a 1D line-space pattern whose size/pitch is 14/28 nm at the wafer scale is used to prove the effectiveness of the proposed model. RCWA, the SDM, and the proposed model are used for calculating the absorber and mask spectrum

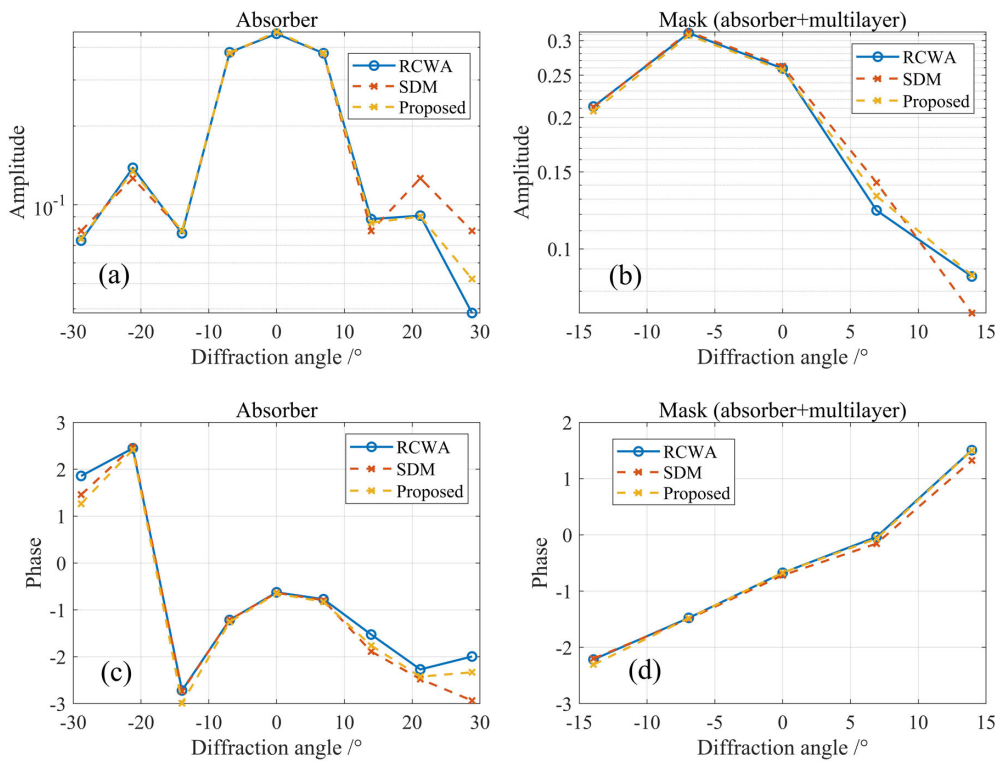


**Fig. 5.** Comparison of RCWA, SDM, and proposed model. (a) Absorber spectrum amplitude. (b) Mask spectrum amplitude. (c) Absorber spectrum phase. (d) Mask spectrum phase.

under TE polarization and 6° incidence angle; the comparison is shown in Fig. 5. The figure shows that the proposed model simulated the absorber diffraction more accurately than the SDM, and resulted in a more accurate calculation of the mask spectrum, especially the +1 and +2 diffraction orders.

### C. 2D Mask Pattern

As shown in Fig. 6, the complex 2D mask patterns are divided into rectangle regions, edges in  $x$  direction, edges in  $y$  direction, and corner points. Then the proposed method can be extended to 2D by applying the 1D frequency domain functions in  $x$  and  $y$  directions, respectively.

Only Manhattan patterns are considered in this paper. With period in  $x$  and  $y$  directions represented by  $p_x$ ,  $p_y$ , the rectangle regions can be described as follows:

$$\left\{ (x, y) \middle| \text{rect} \left( \frac{x - x_{c_i}}{w_{x_i}}, \frac{y - y_{c_i}}{w_{y_i}} \right), i = 1, 2, 3, \dots, s_1 \right\}, \quad (5)$$

where  $s_1$  represents the number of rectangle regions,  $x_{c_i}$  and  $y_{c_i}$  represent the centroid coordinates of the  $i$ -th rectangle region,



**Fig. 6.** Decomposition strategy of 2D mask pattern.

and  $w_{x_i}$  and  $w_{y_i}$  represent the width in  $x$  and  $y$  directions of  $i$ -th region. The edges in  $y$  direction can be described as:

$$\left\{ (x, y) \middle| \delta(x - x_{1i}) \text{rect} \left( \frac{y - y_{c_i}}{w_{y_i}} \right), i = 1, 2, 3, \dots, s_2 \right\}, \quad (6)$$

where  $s_2$  represents the number of edges in  $y$  direction,  $x_{1i}$  represents the abscissa of the  $i$ -th edge,  $y_{c_i}$  represents the midpoint ordinate of the  $i$ -th edge, and  $w_{y_i}$  represents the length of  $i$ -th edge in  $y$  direction. The edges in  $x$  direction can be described as follows:

$$\left\{ (x, y) \middle| \delta(y - y_{1i}) \text{rect} \left( \frac{x - x_{c_i}}{w_{x_i}} \right), i = 1, 2, 3, \dots, s_3 \right\}, \quad (7)$$

where  $s_3$  represents the number of edges in  $x$  direction,  $y_{1i}$  represents the ordinate of the  $i$ -th edge,  $x_{c_i}$  represents the midpoint abscissa of the  $i$ -th edge, and  $w_{x_i}$  represents the length of the  $i$ -th edge in  $x$  direction. The corner points can be described as follows:

$$\left\{ (x, y) \middle| \delta(x - x_i) \delta(y - y_i), i = 1, 2, 3, \dots, s_4 \right\}, \quad (8)$$

where  $s_4$  represents the number of corner points, and  $x_i$  and  $y_i$  represent the coordinate of the  $i$ -th point.

For the mask pattern described by Eqs. (5)–(8), Eq. (3) can be modified to 2D form, as follows:

$$\begin{aligned}
B_{mn} &= t_a \times B_{mn}^{\text{bg}} + (t_b - t_a) \times B_{mn}^{\text{area}} + \frac{A_{\text{pol1}}}{p_x} \times B_{mn}^{y-\text{edge}} \\
&\quad + \frac{A_{\text{pol2}}}{p_y} \times B_{mn}^{x-\text{edge}} + \frac{A_{\text{pol1}} A_{\text{pol2}}}{p_x p_y} \times B_{mn}^{\text{corner}} \\
B_{mn}^{\text{bg}} &= \text{sinc}(m)\text{sinc}(n) \\
B_{mn}^{\text{area}} &= F_{\text{pol1}}(\theta_{x_{\text{eq}}}) d_{x_i} \text{sinc}(m d_{x_i}) F_{\text{pol2}}(\theta_{y_{\text{eq}}}) d_{y_i} \text{sinc}(n d_{y_i}) \\
&\quad \times \exp\left[-2\pi j \left(\frac{m}{p_x} x_{c_i} + \frac{n}{p_y} y_{c_i}\right)\right] \\
B_{mn}^{y-\text{edge}} &= G_{\text{pol1}}(\theta_{x_{\text{eq}}}) d_{y_i} \text{sinc}(n d_{y_i}) \exp\left[-2\pi j \left(\frac{m}{p_x} x_{1_i} + \frac{n}{p_y} y_{1_i}\right)\right] \\
B_{mn}^{x-\text{edge}} &= G_{\text{pol2}}(\theta_{y_{\text{eq}}}) d_{x_i} \text{sinc}(m d_{x_i}) \exp\left[-2\pi j \left(\frac{m}{p_x} x_{c_i} + \frac{n}{p_y} y_{1_i}\right)\right] \\
B_{mn}^{\text{corner}} &= G_{\text{pol1}}(\theta_{x_{\text{eq}}}) G_{\text{pol2}}(\theta_{y_{\text{eq}}}) \exp\left[-2\pi j \left(\frac{m}{p_x} x_{1_i} + \frac{n}{p_y} y_{1_i}\right)\right], \quad (9)
\end{aligned}$$

where  $t_a$ ,  $t_b$ ,  $A$  represent the calibrated model parameters,  $m$  and  $n$  represent the diffraction order in  $x$  and  $y$  directions, and  $d_{x_i}$  and  $d_{y_i}$  represent the duty cycle in  $x$  and  $y$  directions.  $\text{pol}_1$  and  $\text{pol}_2$  represent the polarization modes.  $\text{pol}_1 = \text{TE}$  and  $\text{pol}_2 = \text{TM}$  when polarization is TE, and  $\text{pol}_1 = \text{TM}$  and  $\text{pol}_2 = \text{TE}$  when polarization is TM. Similar to the 1D case,  $\theta_{x_{\text{eq}}}$  and  $\theta_{y_{\text{eq}}}$  represent the “equivalent incidence angles” in  $x$  and  $y$  direction:

$$\begin{aligned}
\theta_{x_{\text{eq}}} &= \frac{\pi}{2} - \arccos(\sin(\theta_{\text{inc}}) \cos(\varphi)) \\
\theta_{y_{\text{eq}}} &= \frac{\pi}{2} - \arccos(\sin(\theta_{\text{inc}}) \sin(\varphi)). \quad (10)
\end{aligned}$$

Then the EUV mask vector spectrum with the 2D pattern can be fast calculated by Eqs. (10) and (1), and the vector imaging model based on Abbe theory is adopted to calculate the aerial image.

### 3. SIMULATION AND ANALYSIS

#### A. Simulation Settings

Dipole illumination as shown in Fig. 7 is used for imaging simulation. The inner and outer sigma factors are 0.3 and 0.8, and the pole angle is 30°. The polarization mode is TE unless otherwise specified. The incidence angle  $\theta$  and the azimuth  $\varphi$  of the chief ray of source are 6° and 0°, respectively. Two reference points at the centroid of the poles are selected to calculate the mask spectrum, and the hybrid Hopkins–Abbe (HHA) method [20] is adopted to simulate the aerial image. The material of the absorber is TaN whose complex index is 0.926 – 0.0436 $j$  and thickness is 70 nm. The multilayer is composed of 40 bilayers of Mo/Si with a thickness of 2.78/4.17 nm. The complex index of Mo and Si is 0.9238 – 0.0064 $j$  and 0.999 – 0.0018 $j$ , respectively. The reduction of projection system is 4×. The multilayer defects and aberration are not considered in this paper. The pitches and sizes of mask pattern are in wafer scale. The RCWA

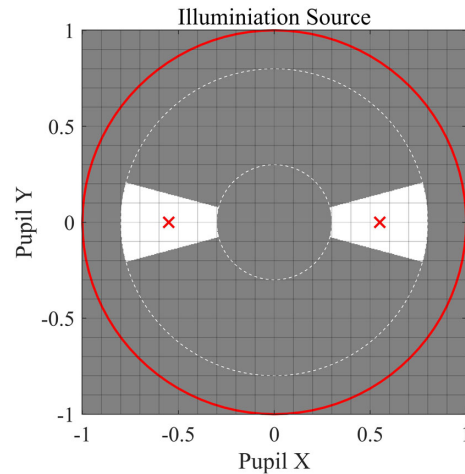


**Fig. 7.** Illumination source.

method is adopted for rigorous simulations, and the SDM is adopted to be the reference fast model. The simulation hardware is a desktop with 8-core 3.6 GHz CPU and 16 GB memory.

#### B. Spectrum Simulation of Line-Space Pattern

Simulations are used to validate that the proposed model can improve the calculation accuracy of the absorber and mask spectrum. For spectrum simulation, normal and oblique illumination represent the incidence directions of the single source point. The sizes/pitches of the line-space mask pattern are set to 125/250 nm, 50/250 nm, 50/100 nm, and 30/100 nm, respectively, under normal illumination. The absorber diffraction spectrum is calculated by RCWA, the SDM and the proposed model; then the calculation error of the spectrum amplitude via two fast models compared to rigorous model are obtained. The amplitude of errors under TE and TM polarizations are shown in Fig. 8.

As shown in Fig. 8, the calculation accuracy of the proposed model is much higher than that of the SDM for different diffraction orders under different feature sizes and polarizations. It proves that the absorber is more accurately modeled by describing the modulation on different orders with frequency domain functions instead of the constant parameters. The root mean square (RMS) values of calculation error for different orders are listed in Table 1:

As shown in Table 1, compared with results of the SDM, the RMS values of the absorber spectrum calculation error obtained by the proposed model reduce more than 78% under various feature sizes. Meanwhile, the calculation error will increase with the decreasing of mask pitch because of the cross talk between the edges, which needs further research.

The incident lights of the second absorber diffraction are from different directions. In order to validate the adaptability of the proposed absorber model for different incidence angles, the size/pitch of pattern is set to 30/100 nm, and the azimuth of incident light is set to 0°; the incidence angles are set to 0°, 5°, 10°, and 15°, respectively. The calculation errors of the SDM and the proposed model are shown in Fig. 9.

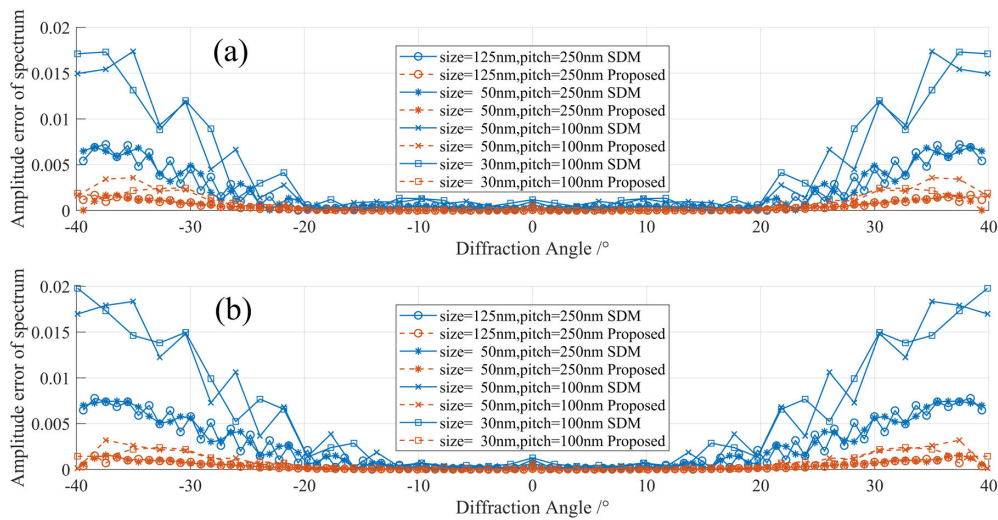


**Fig. 8.** Comparison of calculation errors for absorber spectrum amplitude under different pitch and size. (a) TE polarization. (b) TM polarization.

**Table 1. RMS of Calculation Errors for Absorber Spectrum under Different Pitches and Sizes**

Size/Pitch		125/250	50/250	50/100	30/100
TE	SDM	0.00287	0.00291	0.00741	0.00752
	Proposed	0.00061	0.00059	0.00143	0.00114
	Reduce/%	78.90	79.77	80.74	84.90
TM	SDM	0.00347	0.00348	0.00895	0.00896
	Proposed	0.00052	0.00054	0.00124	0.00109
	Reduce/%	85.10	84.34	86.20	87.86

As shown in Fig. 9, the calculation error of the SDM increases rapidly with the increase of the incidence angle, while the calculation error of the proposed model is much lower. The RMS values of the calculation errors for different orders are listed in Table 2. The RMS values of the proposed model reduce more than 80% for all incidence angles, and the RMS values are

**Table 2. RMS of Calculation Errors for Absorber Spectrum under Different Incidence Angles**

Angle/ $^{\circ}$		0 $^{\circ}$	5 $^{\circ}$	10 $^{\circ}$	15 $^{\circ}$
TE	SDM	0.00752	0.00772	0.00890	0.01095
	Proposed	0.00114	0.00152	0.00104	0.00118
	Reduce/%	84.90	80.28	88.33	89.18
TM	SDM	0.00896	0.00933	0.01042	0.01309
	Proposed	0.00109	0.00134	0.00101	0.00071
	Reduce/%	87.86	85.68	90.32	94.60

almost the same for different incidence angles. This means the model can eliminate the calculation error that resulted from the oblique incidence.

Furthermore, the calculation accuracy of the mask spectrum obtained by the proposed model is validated. Under the condition that the incidence angle is  $6^{\circ}$  and the azimuth is  $0^{\circ}$ , the pattern sizes/pitches are set to 125/250 nm, 50/250 nm,

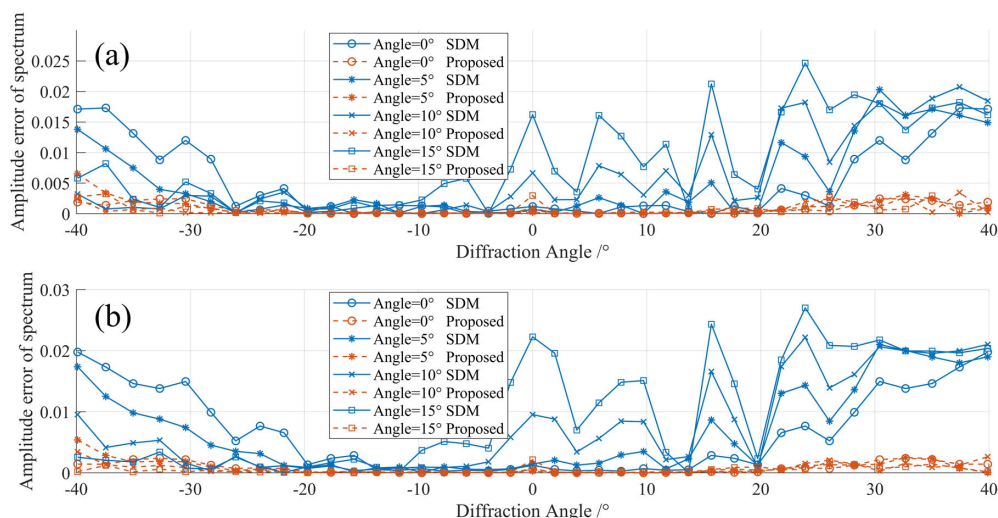


**Fig. 9.** Comparison of calculation errors for amplitude of the absorber spectrum under different incidence angles. (a) TE polarization. (b) TM polarization.

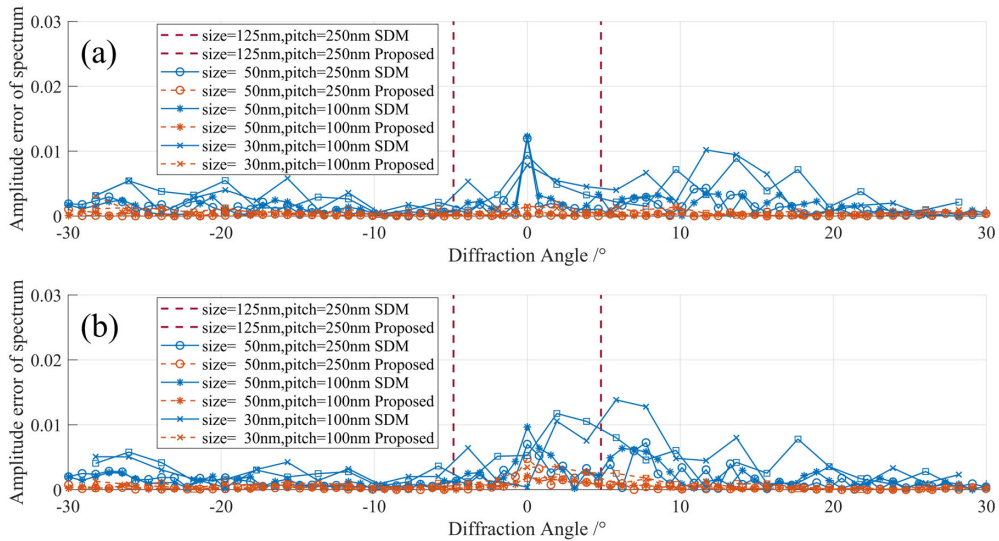


**Fig. 10.** Comparison of calculation errors for mask spectrum amplitude under different pitch and size. (a) TE polarization. (b) TM polarization.

**Table 3. RMS of Calculation Errors for Mask Spectrum under Different Pitches and Sizes**

Size/Pitch (nm)	125/250	50/250	50/100	30/100
TE	SDM	0.00206	0.00222	0.00443
	Proposed	0.00023	0.00030	0.00092
	Reduce/%	88.91	86.32	79.36
TM	SDM	0.00225	0.00261	0.00564
	Proposed	0.00081	0.00056	0.00129
	Reduce/%	63.84	78.71	77.12

50/100 nm, and 30/100 nm, respectively. The mask diffraction spectrum is calculated by RCWA, the SDM, and the proposed model, then the calculation errors are obtained. The amplitude of errors under TE and TM polarizations are shown in Fig. 10.

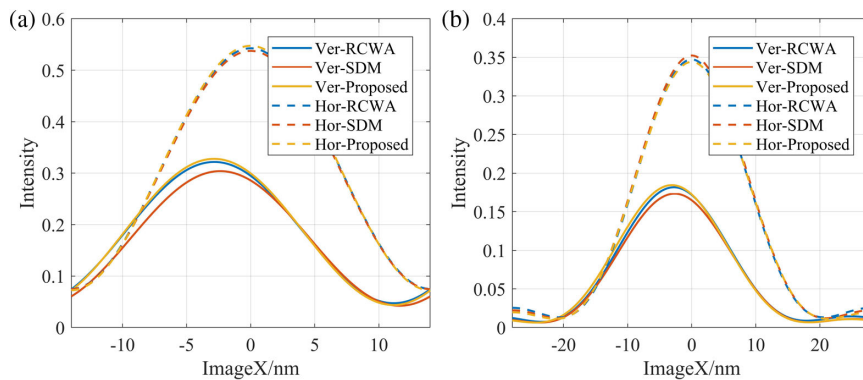
The red dotted lines in the vertical direction, as shown in Fig. 10, represent the filter range of the EUV projection system with 0.33 numerical aperture (NA). As shown in Fig. 10, the calculation errors of the mask spectrum with the SDM are larger than those of the absorber spectrum, especially for low diffraction orders. The reason is that the incident light with the large angle at the second absorber diffraction process also has

an impact on the low diffraction orders of the mask spectrum, while the SDM ignores the impact of oblique incidence on the absorber. The calculation errors of the proposed model are much lower than those of the SDM; the RMS values are listed in Table 3. As we can see, the RMS of the calculation errors reduces more than 60% for features with different sizes, which proves the accuracy of the proposed EUV mask model.

### C. Aerial Image Simulation of Line-Space Pattern

The diffraction lights form the aerial image at the wafer plane via a projection lens. The calculation accuracy of aerial image intensity distribution is key to the resist and etching simulations. In this section, the critical dimension (CD), shadowing effect, and process window of the line-space mask pattern are simulated in order to validate the effectiveness of the proposed mask model on imaging simulations.

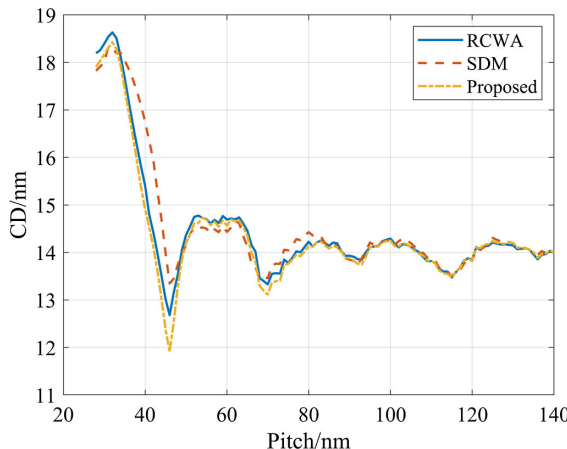
Under the condition that the pattern size is 14 nm and the pitch is 28 nm and 56 nm, respectively, the aerial image is calculated by the RCWA method first. Then the intensity threshold is obtained according to the target CD. The CD values are calculated by the SDM and the proposed model with the threshold, and the calculation error is the difference between the values and



**Fig. 11.** Aerial image intensity of 14 nm line-space pattern. (a) Pitch is 28 nm. (b) Pitch is 56 nm.

**Table 4.** CD Values Calculated by Different Models

Method	H_Dense/nm	V_Dense/nm	H_Iso/nm	V_Iso/nm
SDM	13.81	12.97	14.36	12.84
Proposed	13.95	13.80	14.02	14.07

**Fig. 12.** CD varying with pitches of a 14 nm line-space pattern.

the target CD. The line-space pattern is in the horizon direction when the azimuth of source is  $90^\circ$ , and it is in the vertical direction when the azimuth is  $0^\circ$ . The intensity distributions of aerial images are shown in Fig. 11.

The chief ray angle at object (CRAO) of illumination source is  $6^\circ$ . As shown in Fig. 11, the calculation accuracy of the SDM for the horizon space pattern is pretty high. The reason is that the impact of oblique incidence on the mask spectrum is little when the azimuth is  $0^\circ$ . For a vertical space pattern, the simulation accuracy of the SDM is much lower than that of the proposed model. The CD values calculated by the two fast models are listed in Table 4. The H\_Dense and V\_Dense represent the line-space patterns with pitch being 28 nm in horizon and vertical directions, respectively. The H\_Iso and V\_Iso represent the line-space patterns with pitch being 56 nm in horizon and vertical directions, respectively. For the vertical pattern, the calculation errors of the proposed model are reduced by 80.6%

and 93.9%, respectively, compared with the SDM for dense and isolate features.

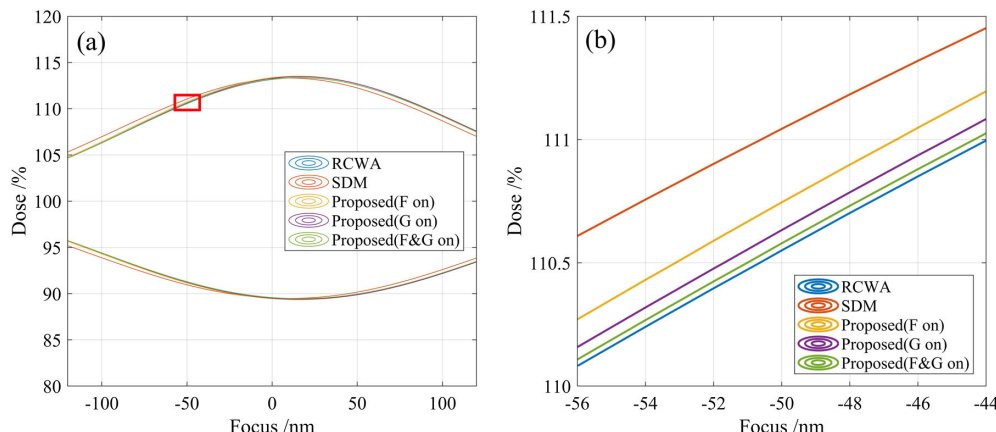
Simulations are performed to evaluate the calculation accuracy of CD values under different mask pitches. For a vertical space pattern with a 14 nm feature, the intensity thresholds are obtained via three models, respectively, with size/pitch being 14/140 nm. Then the CD values under different pitches ranging from 28 nm to 140 nm are calculated, with different threshold values being used for different corresponding models.

As shown in Fig. 12, the CD errors of the proposed model are pretty low. The maximum errors of the proposed model and the SDM are 0.76 nm and 1.55 nm, respectively.

The simulation accuracy of the process window is also very important for a fast model. Under the condition that the size/pitch of vertical space pattern is 14/28 nm, and CD tolerance is  $\pm 10\%$ , the process windows are simulated via different mask models. The reference thresholds are calculated at the 0 nm defocus in advance via different models. For the proposed model, F and G in Eq. (3) are respectively turned on to show their impact on simulation results. As shown in Fig. 13(a), the CD errors calculated via the proposed model are lower than those of the SDM for different defocus values. The best focus is not 0 nm because of the focus shift effect in the EUV imaging system. Figure 13(b) shows the detail of the process window by zooming in on the red rectangular area in Fig. 13(a). It shows that the accuracy of the proposed model is the highest when both F and G are turned on.

The shadowing effect, including the CD bias and pattern shift resulting from the oblique incidence configuration, is important in EUV lithography imaging, which influences the imaging performance. Under the condition that the size/pitch is 15/30 nm, the intensity threshold is calculated by the RCWA method with azimuth being  $90^\circ$ . Then CD values and pattern shift values are calculated via different mask models with azimuths ranging from  $0^\circ$  to  $90^\circ$ .

As shown in Fig. 14, the simulation accuracy of the shadowing effect via the proposed model is higher than that of the SDM. The simulation results of RCWA are used as the benchmark. The maximum calculation error of CD bias via the SDM reaches 2.4 nm, while the maximum error of the proposed model is only 0.3 nm. The calculation error of CD bias via the proposed model changes little with the variation of

**Fig. 13.** Process window calculated by different model. (a) Dose varying with focus. (b) Plot of the red rectangular area in (a).

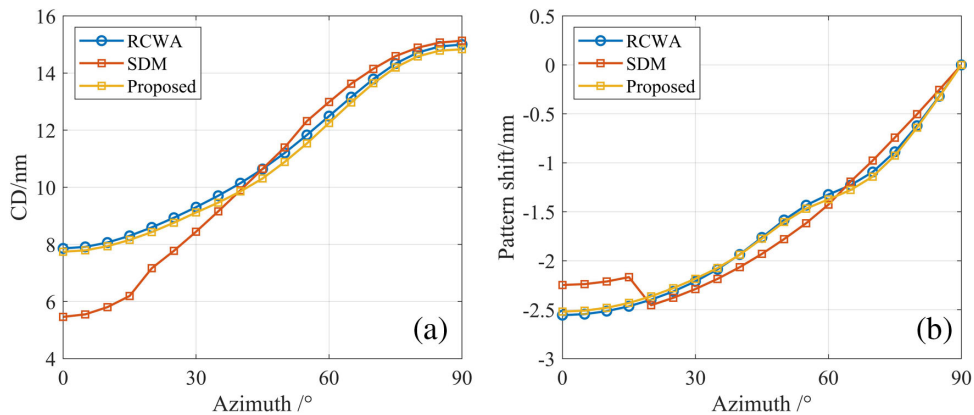


**Fig. 14.** Simulations of shadowing effect by different models. (a) Pattern CD bias. (b) Pattern shift.

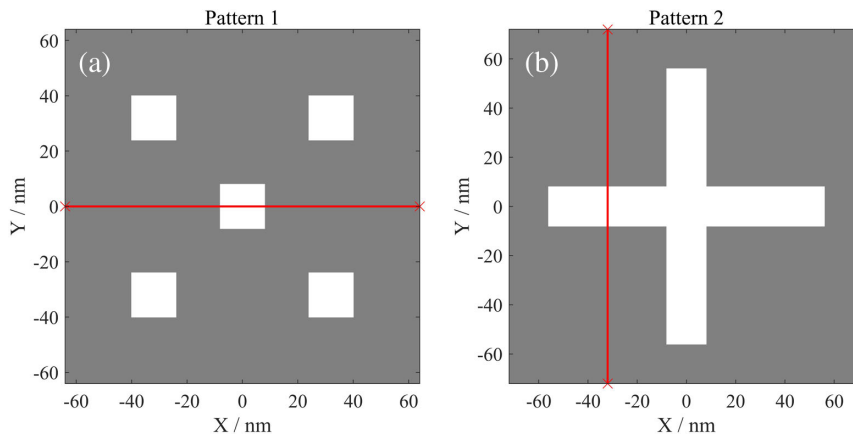


**Fig. 15.** 2D test patterns. (a) Contact holes. (b) Cross pattern.

azimuth, which means the impact of oblique incidence on aerial image can be well described by the proposed model. The maximum calculation error of pattern shifts via the SDM reaches 0.4 nm, while the maximum error of the proposed model is only 0.05 nm. The center position of the aerial image is mainly determined by the phase of mask spectrum. This means that calculation accuracy is improved by the proposed model for both the amplitude and phase of mask spectrum.

Based on the simulation results and analysis in Sections 3.A and 3.B, the simulation accuracy of the proposed model on mask spectrum, CD values, shadow effects, and process window are almost the same as that of the traditional rigorous model for a 1D mask pattern. On the other hand, the fundamental of the proposed model is structure decomposition, so the calculation speed is much higher than that of the RCWA method, which makes the proposed model a fast rigorous EUV mask model.

#### D. Aerial Image Simulation of 2D Pattern

The actual circuit patterns are generally 2D Manhattan pattern. To validate the adaptability of the proposed model for 2D mask patterns, two test patterns including contact holes and cross pattern are used for simulations of aerial image. In 2D cases, the illumination source condition remains the same with the 1D cases.

Test pattern 1 is composed of five contact holes whose length and width are both 22 nm, and mask pitches are 128 nm in  $x$  and  $y$  directions. Test pattern 2 is a cross pattern, which is formed by two rectangles perpendicular to each other. The length and width of the rectangle are 16 nm and 112 nm, respectively, and the mask pitch is 144 nm in  $x$  and  $y$  directions. The numbers of diffraction orders in  $x$  and  $y$  directions are set to  $17 \times 17$  and  $23 \times 23$  for two patterns, respectively. The red lines in Fig. 15 are cutlines to calculate the threshold and CD.

RCWA, the SDM, the DDM, and the proposed model are used to simulate the aerial images of the test patterns. The aerial images normalized by maximum value are shown in Fig. 16. The calculation errors between the two fast models and the rigorous model are shown in Fig. 17.

As we can see, the simulation accuracy of the proposed model is higher than that of the SDM and DDM for both test patterns. The RMS values of calculation errors using the SDM for the two patterns are 0.054 and 0.0205. The RMS values of the DDM are 0.0283 and 0.0241, and the RMS values of the proposed model are just 0.0109 and 0.0091. The RMS values have been reduced by 79.8% and 55.6% compared with that of the SDM, and have been reduced by 61.5% and 62.2% compared with that of the DDM. This proves that the proposed model can effectively improve the simulation accuracy of a 2D mask pattern.

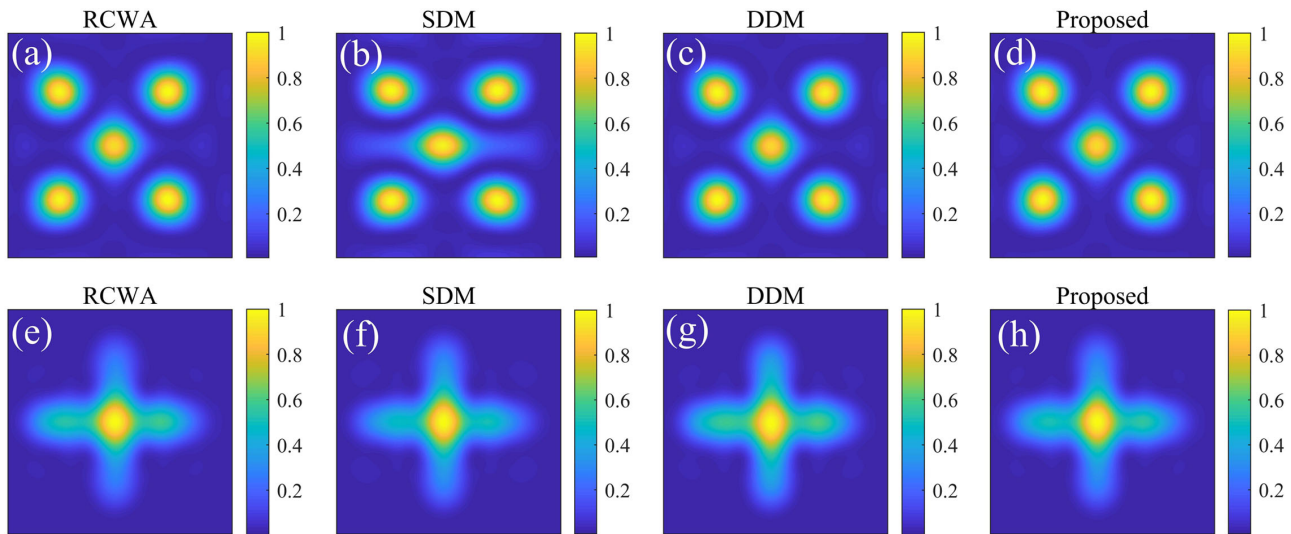


**Fig. 16.** Aerial image intensities calculated by different models. (a)–(d) are results of pattern 1. (e)–(h) are results of pattern 2.

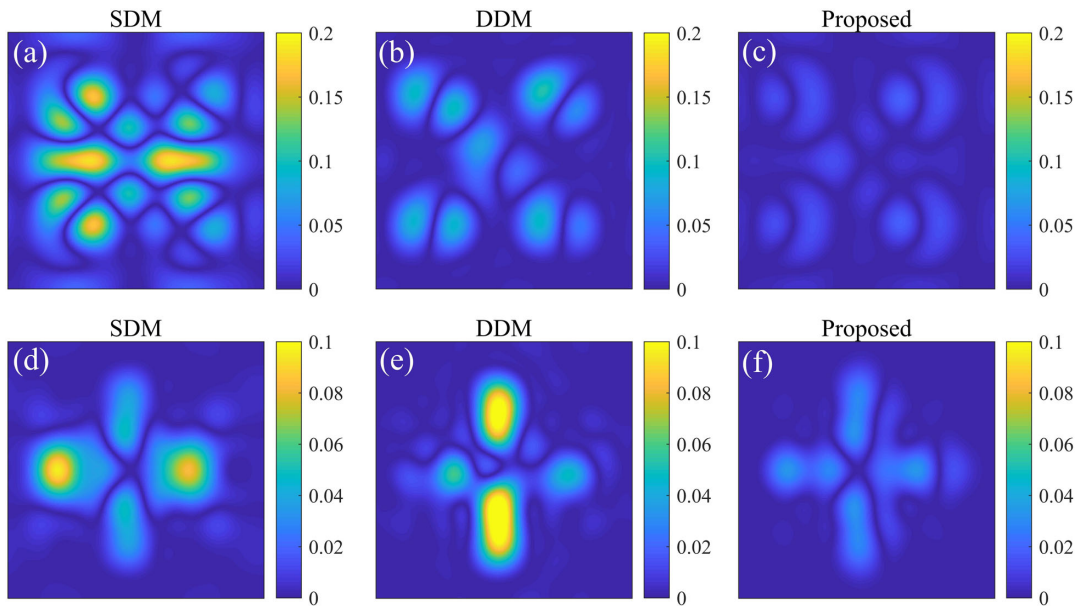


**Fig. 17.** Calculation errors of SDM and proposed model. (a)–(c) are results of pattern 1. (d)–(f) are results of pattern 2.

**Table 5. Runtime and CD Values Comparison of Different Models**

Method	RCWA	SDM	DDM	Proposed
Pattern 1/nm	22	28.4	21.4	21.5
Error/nm	/	6.4	0.6	0.5
Runtime/s	24.6	0.14	0.15	0.25
Pattern 2/nm	16	12.85	17.78	15.17
Error/nm	/	3.15	1.78	0.83
Runtime/s	125.8	0.2	0.24	0.32

The intensity distributions at the cutlines calculated by RCWA are extracted to obtain the thresholds to target CD first, which are 0.5203 and 0.3863, respectively. Then the CD values are calculated by two fast models and are listed in Table 5.

As we can see, the calculation errors of CD by the proposed model reduce sharply compared with the SDM and the DDM. Compared with the RCWA rigorous method, the simulation errors are only 0.5 nm and 0.83 nm, and the calculation runtime is reduced by 98.9% and 99.7% for the two test patterns, respectively. Although additional runtime is needed because of the interpolation of the library data, the runtimes of the proposed model are in the same order of magnitude compared with the SDM and the DDM. Furthermore, the runtime of the rigorous model will increase rapidly with the increasing of diffraction orders, while it has little impact on the calculation speed of the proposed model.

Finally, with the threshold being 0.5203 and 0.3863, the 2D resist contours are obtained. As shown in Fig. 18, the resist

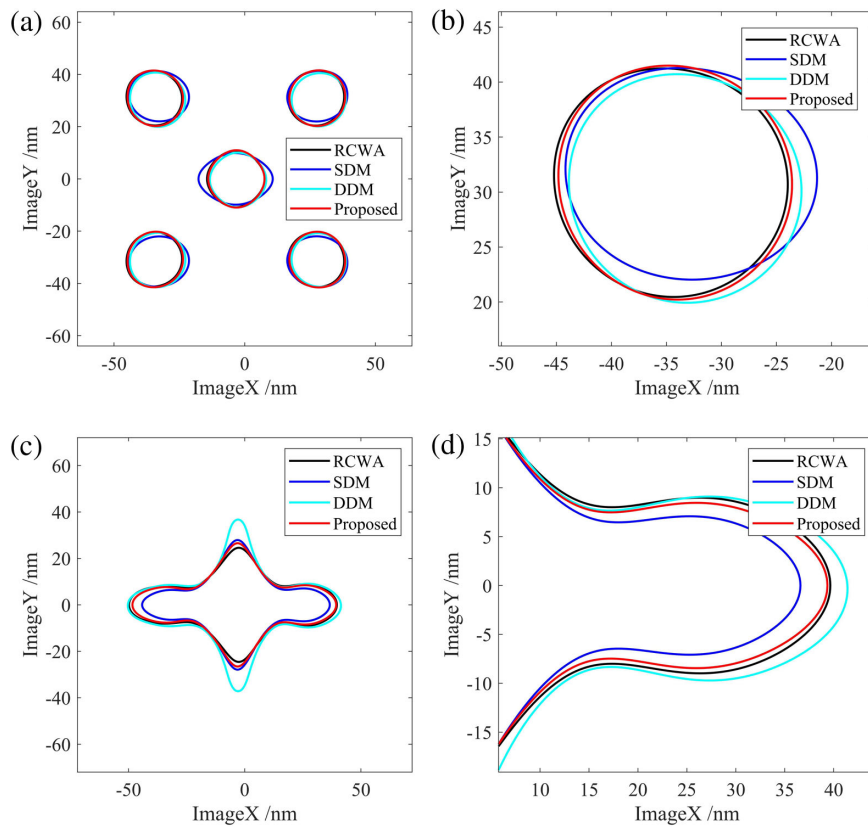


**Fig. 18.** Resist contours obtained by different models. (a) Test pattern 1. (b) Detail of the yellow rectangular area in (a), (c) test pattern 2, (d) detail of the yellow rectangular area in (c).

contours calculated by the proposed model are almost the same as that calculated by the RCWA rigorous method.

Based on the simulations and analysis in Section 3.C, although the proposed model for the 2D case is obtained by the extension of the model for the 1D pattern, the simulation accuracy of the proposed model remains pretty high, almost the same as that of the traditional rigorous model. Meanwhile, the simulation runtime of the proposed model is much lower than that of the traditional rigorous model. The proposed model realizes fast rigorous simulation of the mask spectrum.

#### 4. CONCLUSION

A fast and rigorous EUV mask model has been proposed in this paper, which accurately simulates the diffraction spectrum of the EUV mask. Fast imaging simulation is realized with the proposed mask model and vector imaging model. Frequency domain functions are adopted to accurately calculate the absorber spectrum, mask spectrum, and aerial image of the line-space pattern with arbitrary incidence angles. Both 1D and 2D patterns are employed in simulations to verify the validity of the proposed model. Simulation results show that the simulation accuracy of the aerial image, CD values, shadowing effect, and process window are all improved by the proposed model compared to the SDM. For the 14 nm vertical line-space pattern, the CD errors calculated by the proposed model are reduced by 80.6% and 93.9% compared with the SDM for dense and isolate features. The simulation accuracy of the proposed model

is almost the same as that of the rigorous model, while simulation speed is improved significantly compared with the rigorous model. The accuracy of the proposed model mainly depends on the feature size. When the features on the mask layout are pretty small, and the distances of the features decrease, the accuracy of the proposed model will decrease because of the severe cross-talk effect between the edges. Further research will be focused on the fast models for the EUV mask with edges inclination and non-Manhattan patterns.

**Funding.** National Science and Technology Planning Project (2012ZX02702001-006, 2017ZX02101004-002); Natural Science Foundation of Shanghai (17ZR1434100).

**Acknowledgment.** The authors thank Dr. Heng Zhang and Dr. Yanjie Mao for their valuable suggestions.

**Disclosures.** The authors declare no conflicts of interest.

#### REFERENCES

1. S. S. Kim, R. Chalykh, and H. Kim, "Progress in EUV lithography toward manufacturing," *Proc. SPIE* **10143**, 1014306 (2017).
2. X. Ma, Z. Wang, Y. Li, G. R. Arce, L. Dong, and J. Garcia-Frias, "Fast optical proximity correction method based on nonlinear compressive sensing," *Opt. Express* **26**, 14479–14498 (2018).
3. Y. Shen, F. Peng, X. Huang, and Z. Zhang, "Adaptive gradient-based source and mask co-optimization with process awareness," *Chin. Opt. Lett.* **17**, 121102 (2019).

4. X. Wu, S. Liu, J. Li, and E. Y. Lam, "Efficient source mask optimization with Zernike polynomial functions for source representation," *Opt. Express* **22**, 3924–3937 (2014).
5. S. Li, X. Wang, and Y. Bu, "Robust pixel-based source and mask optimization for inverse lithography," *Opt. Laser Technol.* **45**, 285–293 (2013).
6. C. Yang, S. Li, and X. Wang, "Efficient source mask optimization using multipole source representation," *J. Micro/Nano. MEMS MOEMS* **13**, 043001 (2014).
7. P. Evanschitzky and A. Erdmann, "Advanced EUV mask and imaging modeling," *J. Micro/Nano. MEMS MOEMS* **16**, 041005 (2017).
8. A. Vial, A. Erdmann, T. Schmoeller, and C. Kalus, "Modification of boundaries conditions in the FDTD algorithm for EUV mask modeling," *Proc. SPIE* **4754**, 890–899 (2002).
9. Z. Zhu, K. Lucas, J. Cobb, S. Hector, and A. Strojwas, "Rigorous EUV mask simulator using 2D and 3D waveguide methods," *Proc. SPIE* **5037**, 494–503 (2003).
10. M. Lam, K. Adam, D. Fryer, and C. Zuniga, "Accurate 3DEMFI mask model for full-chip simulation," *Proc. SPIE* **8683**, 86831D (2013).
11. K. Adam and A. Neureuther, "Methodology for accurate and rapid simulation of large arbitrary 2D layouts of advanced photomasks," *Proc. SPIE* **4562**, 1051–1067 (2002).
12. P. Liu, X. Xie, W. Liu, and K. Gronlund, "Fast 3D thick mask model for full-chip EUVL simulations," *Proc. SPIE* **8679**, 86790W (2013).
13. Y. Cao, X. Wang, A. Erdmann, P. Bu, and Y. Bu, "Analytical model for EUV mask diffraction field calculation," *Proc. SPIE* **8171**, 81710N (2011).
14. S. Raghunathan, G. McIntyre, G. Fenger, and O. Wood, "Mask 3D effects and compensation for high NA EUV lithography," *Proc. SPIE* **8679**, 867918 (2013).
15. J. Mailfert, C. Zuniga, V. Philipsen, K. Adam, M. Lam, and J. Word, "3D mask modeling for EUV lithography," *Proc. SPIE* **8322**, 832224 (2012).
16. S. Lan, J. Liu, Y. Wang, K. Zhao, and J. Li, "Deep learning assisted fast mask optimization," *Proc. SPIE* **10587**, 105870H (2018).
17. X. Liu, X. Wang, S. Li, G. Yan, and A. Erdmann, "Fast rigorous model for mask spectrum simulation and analysis of mask shadowing effects in extreme ultraviolet lithography," *Proc. SPIE* **9048**, 90483E (2014).
18. X. Liu, S. Li, and X. Wang, "Simulation model based on equivalent layer method for defective mask multilayer in extreme ultraviolet lithography," *Acta Opt. Sin.* **35**, 0622005 (2015).
19. J. Finders, L. Winter, and T. Last, "Mitigation of mask three-dimensional induced phase effects by absorber optimization in ArFi and extreme ultraviolet lithography," *J. Micro/Nano. MEMS MOEMS* **15**, 021408 (2016).
20. K. Adam and M. Lam, "Hybrid Hopkins-Abbe method for modeling oblique angle mask effects in OPC," *Proc. SPIE* **6924**, E9241 (2008).